King Saud University

Arabian Journal of Chemistry

www.ksu.edu.sa
www.sciencedirect.com

ORIGINAL ARTICLE

Engineered biochar derived from lemon peel waste for highly efficient removal of organic pollutants from water

Zhijuan Li, Miya Zhou, Ningxin Liu, Fuyan Zhang, Keyao An, Xinwei Xiong, Shuangyan Fan, Qi Sun *, **Tao Le** *

College of Life Sciences, Chongqing Normal University, No.37 Chengzhong Road, Shapingba District, Chongqing 401331, People's Republic of China

Abstract The urgent need for efficient decontamination of organic dyes from polluted waters necessitates the search for a low-cost and suitable adsorbent. The large amount of lemon peel residue in actual production can be an ideal raw material for the preparation of adsorbents. Herein, a novel magnetic nanocomposite derived from lemon (*Citrus limon L.*) peel residue (Fe_3O_4/Lp-biochar) was successfully synthesized by one-step hydrothermal method and used for the adsorptive capture of methylene blue (MB) in aqueous solution. The prepared Fe_3O_4/Lp-biochar are spherical with a particle size of 8.3 nm and have a saturation magnetization intensity of 52.9 emu/g and a specific surface area of 64.30 m^2/g. It was found that the maximum MB adsorption capacity of 26.36 mg/g by the Fe_3O_4/Lp-biochar can be achieved when the amount of nanocomposite was 0.10 mg/mL, the system's pH value was 10, the reaction temperature was 25 °C, and the adsorption time was 60 min. Adsorption kinetics of MB on the Fe_3O_4/Lp-biochar followed the pseudo-second-order kinetic model whilst the Freundlich isotherm model could well simulate the adsorption behavior of MB on magnetic biochar. The adsorption mechanism of MB by the Fe_3O_4/Lp-biochar predominantly include electrostatic attraction and mesoporous interaction. Furthermore, the Fe_3O_4/Lp-biochar exhibited a remarkable retention of 94.7% of the initial adsorption efficiency even after the 10th cycle of repeated use. It was

* Corresponding author.
 E-mail addresses: sunqi2017@cqnu.edu.cn (Q. Sun), letao@cqnu.edu.cn (T. Le).
Peer review under responsibility of King Saud University.

Production and hosting by Elsevier

concluded that the lemon peel-derived magnetic biochar can be a promising alternative to conventional adsorbents for wastewater treatment.

1. Introduction

The development of chemical industries increased the contamination of water bodies with diverse organic pollutants, causing a serious environmental problem (Behin and Farhadian 2017, Ghabaee et al., 2020, Pourzad et al., 2020). Over 100, 000 commercially available dyes with over 7×10^5 tons of dyestuff are produced annually worldwide (Benjelloun et al., 2021). However, 10–15% of dyestuff is estimated to be discharged into the aquatic environment (Zhou et al., 2019). Among dyestuffs, methylene blue (MB)-IUPAC name: [7-(dimethylamino) phenothiazin-3-ylidene]-dimethylazanium chloride, is a representative organic compound of water-soluble dyes and is extensively used in industries (Albishri and Katouah 2023). Wastewater containing MB can often damage the natural environment and human health (Nabilah et al., 2023). Therefore, the pretreatment of dye-containing wastewater before its discharge to the surrounding is a very important issue and has attracted worldwide attention.

Adsorption using low-cost adsorbents in this context has been one of the most promising methods for dye removal from wastewaters due to the efficiency, easiness, and sustainability (Ebrahimzadeh and Behbahani 2017, Sobhi et al., 2022, Davoodbeygi et al., 2023). Nevertheless, most of the adsorbents used in wastewater treatment so far have been petroleum-derived carbon materials. In comparison with traditional activated carbon, biochar is a promising renewable carbonaceous material produced by biological waste pyrolysis with abundant pore structure, and it is recently used in sensing detection, energy, and environmental areas (Harindintwali et al., 2023, Yin et al., 2023). For example, researchers developed an electrochemical sensor modified with walnut shell-derived biochar for simultaneous detection of heavy metal ions in water and soil samples (El Hamdouni et al., 2022). The use of biochar to produce renewable energy is considered a sustainable approach to creating an energy secure world, and research work on this topic has been extensively reviewed in recent years (Kant Bhatia et al., 2021, Awasthi 2022). In addition, biochar has become emerging adsorbent for achieving environmental-friendly remediation due to its various sources, abundant surface functional groups, high porosity and low cost. Researchers have studied the potential of diverse biomass-derived biochar, such as oil palm frond (Sutarut et al., 2023) or *Eichhornia crassipes* based biochar products (Wu et al., 2023) for mixed pollutants adsorption potential from real industrial wastewater. The separation of biochar powder from environmental media often necessitates additional steps such as centrifugation and filtration. However, these steps can limit the applications of biochar and potentially contribute to secondary pollution. Thus, Relevant studies have been conducted to investigate the use of magnetism in sorbents as an efficient recovery strategy.

Magnetic biochar can be obtained through the combination of magnetic materials and biochar using processes as pyrolytic activation and chemical co-precipitation (Qu et al., 2020, Peng et al., 2022). Compared with conventional biochar, magnetic biochar not only retains the excellent characteristics but also possesses the additional feature of magnetic separation. As an important magnetic material, magnetite nanoparticles (Fe_3O_4 NPs) have become a desirable option for rapid magnetic separation. Jung et al. (2016) have synthesized a magnetic biochar/Fe_3O_4 nanocomposite from marine macroalgae and demonstrated that the magnetic biochar has superior removal efficiency for acid orange than nonmagnetic biochar due to its simultaneous improvement in porosity and functionality. Although the separation of magnetic biochar from aqueous solutions is favorable, the adsorp-

tion performance of magnetic biochar for pollutants is limited, and the research on magnetic biochar is still in the development stage (Qu et al., 2022).

Lemon (*Citrus limon L.*), an internationally important fruit crop, is widely grown in Chongqing, China. In Tongnan District, for example, the cultivation area of lemons has almost doubled from 2015 to 2020, leading to an increase in lemon production from 180,000 tons to 280,000 tons. As one of the important by-products of lemon processing, lemon peel accounts for about 20% of the whole fruit and can be used for the preparation of biochar materials, thus avoiding environmental pollution and resource waste (Jiang et al., 2022).

On account of the aforementioned analyses, this study attempts to i) investigate the possibility and feasibility of producing magnetic biochar nanocomposites by hydrothermal carbonization of lemon peel as a raw material at low temperatures; ii) assess the adsorption capacity of the magnetic lemon peel-derived biochar nanocomposite (denoted as Fe_3O_4/Lp-biochar) for methylene blue (MB) under different operational conditions; iii) provide insights into the adsorption isotherm and kinetic models, as well as the adsorption mechanism. This study provides a new way for the high value scientific utilization of lemon peel residue, and also has important reference value for the related research in the environmental field.

2. Materials and methods

2.1. Materials

Lemon (*Citrus limon L.*) peel wastes were obtained from a lemon processing plant in Tong-nan District, Chongqing, China. The collected lemon peels were subsequently dried, pulverized and sifted through a 20-mesh sieve. Ferric chloride hexahydrate ($FeCl_3 \cdot 6H_2O$), urea and anhydrous ethanol ($\geq 99.7\%$) were purchased from Aladdin Co., Ltd (Shanghai, China) and were of analytical reagent pure. The MB dye powder was bought from Sigma-Aldrich. Ultra-pure water was obtained using a Milli-Q system (Millipore, Bedford, MA) and used throughout all experiments.

2.2. Preparation and characterization of magnetic biochar adsorbent

In an optimal condition, 2.0 g of the as-prepared lemon peel powder, 200 mg of $FeCl_3 \cdot 6H_2O$ and 600 mg of urea were added into 30 mL of deionized water with stirring. The formed homogeneous solution was then transferred to a 50 mL Teflon-lined stainless-steel autoclave, placed at 180 °C for 15 h, removed and cooled to room temperature. The resulting black product was collected by magnetic separation, washed with deionized water, and vacuum-dried at 40 ℃ for 12 h.

The structure morphology of as-synthesized magnetic biochar adsorbent (denoted as Fe_3O_4/Lp-biochar) was identified by Quanta FEG 650 scanning electron microscopy (SEM) and FEI Tecnai G2 F20 transmission electron microscopy (TEM), respectively. X-Ray diffraction (XRD) and Fourier

transform infrared (FT-IR) spectra of Fe_3O_4/Lp-biochar were recorded using Rigaku D/Max-2400 X-ray diffractometer (Rigaku, Japan) and IFS120HR Fourier transform infrared spectroscopy (Bruker, German), respectively. Thermogravimetric analysis (TGA) was conducted to analyze the thermal properties of biochar samples using an STA 449C thermogravimetric analyzer (Netzsch, German). The Brunauer-Emmett-Teller (BET) specific surface area of the nanocomposite was detected using an ASAP2020 automatic gas-adsorption analyzer (Micromeritics, USA). For magnetic measurements, the magnetic hysteresis loop of Fe_3O_4/Lp-biochar was recorded on a PPMS model vibrating sample magnetometer (VSM) at 25 °C in a magnetic field range from − 10,000 to 10,000 Oe. The ultraviolet–visible (UV–vis) absorption spectra were tested with a UH5300 UV–vis spectrophotometer (Hitachi, Japan) with a standard quartz cell (1.0 cm path length).

2.3. Batch adsorption experiments

The adsorption of MB was performed in a shaker at 300 rpm and room temperature. Several operational factors were evaluated to determine their effects on MB adsorption efficiency. For the optimal mass of sorbent, 10 mL of MB solution with 10 mg/L was spiked with various concentrations of Fe_3O_4/Lp-biochar (0.01–0.20 mg/mL). The influence of the solution pH on the adsorption capacity was studied by varying the initial pH between 2 and 10. To evaluate the effect of initial dye concentration on the adsorption efficiency, 10 mL of MB solution with initial concentrations of 5–50 mg/L were shaken with 10 mg of Fe_3O_4/Lp-biochar. The adsorption efficiencies of Fe_3O_4/Lp-biochar for different MB concentrations within 6 h were also investigated, and the influence of temperature was further analyzed at 20–45 ℃. For all batch experiments, the suspension (0.2 mL) was separated from the reaction system using a magnet, and the equilibrium concentrations of MB were determined by UV–vis spectroscopy at the maximum absorption wavelength. The removal efficiency and adsorption capacity of MB on Fe_3O_4/Lp-biochar were quantified using Eqs. (1) and (2), as follows:

$$R = \frac{(C0 - Ceq)}{C0} \times 100 \qquad (1)$$

$$q_e = \frac{(C0 - Ceq)V}{m} \qquad (2)$$

where R (%) and q_e (mg/g) represent the removal percentage and the equilibrium capacity of MB absorbed on Fe_3O_4/Lp-biochar, respectively. C_0 and C_{eq} are the initial and equilibrium concentrations of the MB solution, respectively. V (L) is the total volume of MB solution, and m (g) is the mass (g) of biochar powder used in the absorption experiment.

2.4. Adsorption kinetic studies

In order to deeply understand the kinetic process of MB absorption on Fe_3O_4/Lp-biochar, pseudo-first-order kinetic, pseudo-second-order kinetic, Freundlich isotherm and particle diffusion kinetic models were used to fit the obtained experimental data linearly.

2.5. Reusability evaluation

Briefly, when adsorption equilibrium was reached, 10 mL of anhydrous ethanol was added to the magnetically separated Fe_3O_4/Lp-biochar and the pH of the reaction system was adjusted to 2 with 0.1 M HCl, followed by incubation at 300 rpm for 1 h. After magnetic separation, the obtained Fe_3O_4/Lp-biochar was washed several times with deionized water and absolute ethanol. The collected adsorbents were dried at 60 ℃ for 2 h in a vacuum drying oven and used for further adsorption–desorption experiments. To evaluate the stability and reusability of Fe_3O_4/Lp-biochar, regeneration cycles were conducted ten times at optimum adsorption conditions.

3. Results and discussion

3.1. Characterization of Fe_3O_4/Lp-biochar

The SEM (Fig. 1 A) and TEM (Fig. 1B) images showed that the as-obtained Fe_3O_4/Lp-biochar nanocomposite had a globular shape with homogeneous size distribution. Notably, the core–shell structure can further prevent the aggregation of Fe_3O_4 nanoparticles. The energy dispersive X-ray spectroscopy (EDS) coupled with SEM showed that C and Fe_3O_4 were present at 48.31% and 51.57%, respectively. Meanwhile, XRD was used to detect the crystalline structure of Fe_3O_4/Lp-biochar (Fig. 1 C). The X-ray diffraction peaks at 2θ = 30.1°, 35.4°, 43.1°, 53.4°, 57.1°, 62.5° corresponding to the (220), (311), (400), (422), (511) and (440) reflection planes coincided with the cubic phase of Fe_3O_4 (Bhattacharya et al., 2015). The biochar adsorbent displayed a broad diffraction peak at around 22°, which is related to the (002) crystal plane of the carbon materials (Liu et al., 2019). The FTIR spectrum analysis (Fig. 1 D) showed characteristic peaks at 3340, 2930, 1700 and 1320 cm^{-1}confirming the presence of O–H, C–H, C = O and C = C groups, respectively, related to the carbonization of sugar substances such as pectin contained in the lemon peel. The characteristic absorption peak at 573 cm^{-1}confirmed the Fe-O stretching vibrations of Fe_3O_4 (Chae et al., 2015).

The Fe_3O_4/Lp-biochar did not exhibit magnetic hysteresis at room temperature (Fig. 2A). The curve displayed a saturation magnetization of 52.9 emu/g with characteristic superparamagnetic behavior, indicating that the magnetic adsorbent was successfully prepared. The inset in Fig. 2A showed that Fe_3O_4/Lp-biochar maintained its good dispersity in aqueous solutions, and the external magnetic field can then be used to realize the adsorbent in duplicates. The profile of TGA curves (Fig. 2B) demonstrated weight loss in three stages for Fe_3O_4/Lp-biochar between 25 and 650 ℃. The first stage of TGA usually involves mass loss due to water evaporation, corresponding to the initial weight loss below 200 ℃. During the second stage, a sharp mass loss occurred due to the the oxidation of the amorphous carbon shell between 200 and 400 ℃. No significant mass change was observed in the range of 500 ~ 650 ℃ as previously reported (Xuan et al., 2007). Besides, the nitrogen adsorption–desorption curve (Fig. 2C) revealed that Fe_3O_4/Lp-biochar followed a typical type-IV isotherm with a hysteresis-loop above P/P_0 = 0.8, indicating the existence of mesopores in the samples. The pore size distribu-
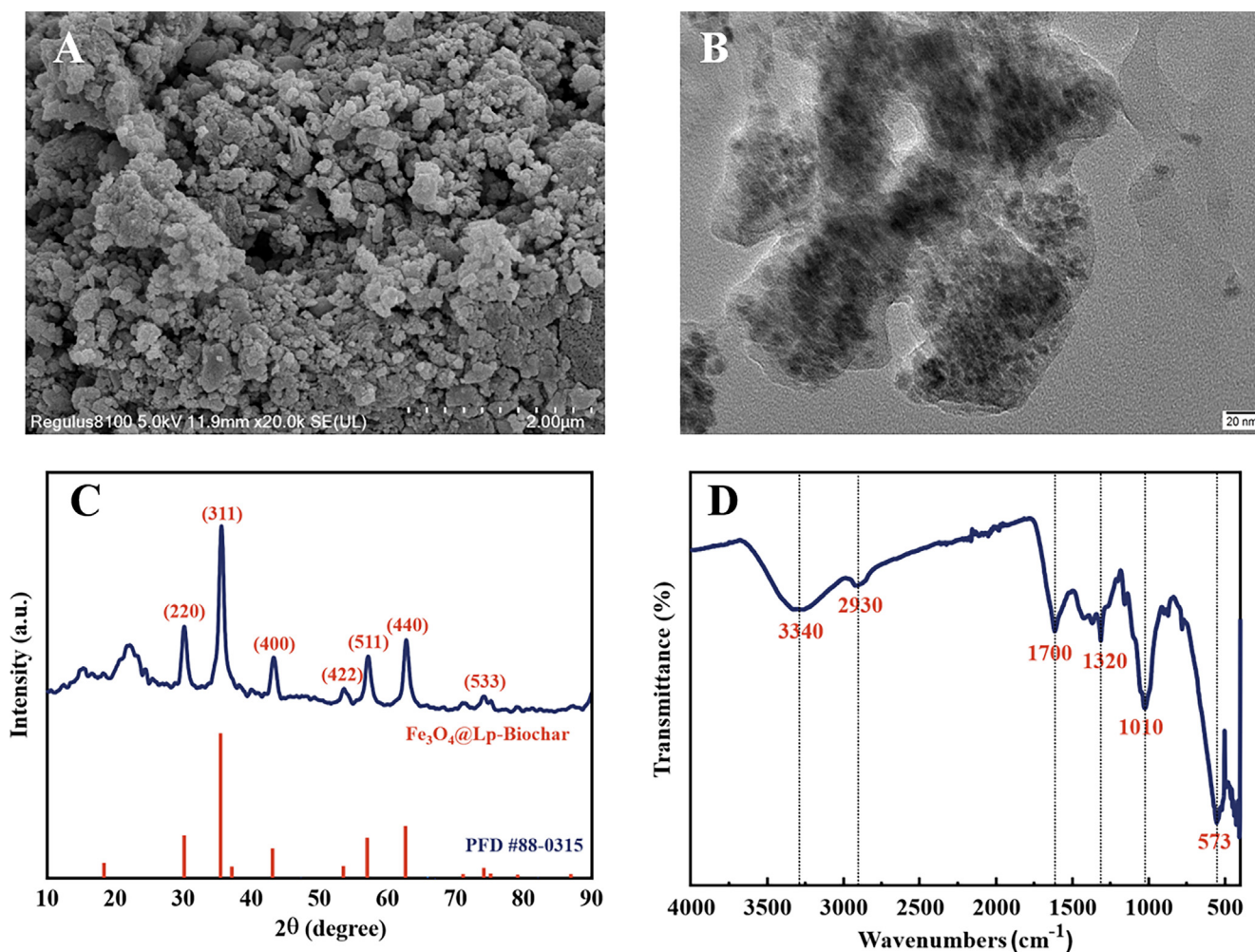
Fig. 1 (A) SEM and (B) TEM images of magnetic biochar nanocomposite namely with Fe_3O_4/Lp-biochar derived from lemon (*Citrus limon L.*) peel waste. (C) XRD and (D) FTIR patterns of the Fe_3O_4/Lp-biochar.

tion of mesopores ranged from 15 to 50 nm (Fig. 2D). Furthermore, nitrogen adsorption/desorption measurement revealed a specific surface area of 64.30 m²/g for Fe_3O_4/Lp-biochar, which was higher than other reported values (Lan et al., 2014, Mao et al., 2014, Pu et al., 2014).

3.2. Mechanism of Fe_3O_4/Lp-biochar formation

The formation mechanism of lemon peel derived biochar adsorbent is discussed below. Lemon peel is rich in polysaccharides, such as pectin and flavonoids, which are generally hydrolyzed to monosaccharides (e.g., galactose, arabinose and glucose) under alkaline conditions (Ivanova et al., 2012). Moreover, urea can provide an alkaline environment for Fe_3O_4 NPs formation under hydrothermal conditions (Xuan et al., 2007, Zhang et al., 2016). First, Fe^{3+} ions in the reaction system can be partly reduced to Fe^{2+} by some monosaccharides, and then the concentrated nucleation sites for Fe_3O_4 NPs are formed via the dehydration of these ions. The rich carboxyl groups in the lemon peel will form cross-linking with Fe^{2+} and Fe^{3+} ions on the surface of Fe_3O_4 NPs, preventing the agglomeration of magnetic nanoparticles (Kyomugasho et al., 2015). Next, a reactive surface would exist in the

Fe_3O_4 NPs. These carbon species generated from the carbonization of pectin and other derivatives in the lemon peel can adhere to the exposed surface, resulting in the biochar-coated Fe_3O_4 NPs (Fe_3O_4/Lp-biochar).

3.3. Adsorption capacity of Fe_3O_4/Lp-biochar

Herein, methylene blue (MB) dye was used to explore the adsorption properties of the as-synthesized Fe_3O_4/Lp-biochar. The adsorption efficiency of Fe_3O_4/Lp-biochar to MB increased with the increasing pH values in the range of $2 \sim 10$ primarily due to the electrostatic interaction between biochar adsorbent and MB dye in different pH conditions. The reason was that the isoelectric point (pI) of the Fe_3O_4/Lp-biochar was 3.6. When the solution pH was higher than pI, the surface of the Fe_3O_4/Lp-biochar is negatively charged, which promoted the adsorption of cationic MB dyes. The reason was that MB adsorption was primarily controlled by electrostatic interaction between dye molecules and the surface of Fe_3O_4/Lp-biochar.

The initial MB concentration was also an important factor influencing the sorption efficiency. The adsorption capacity of the Fe_3O_4/Lp-biochar at equilibrium significantly
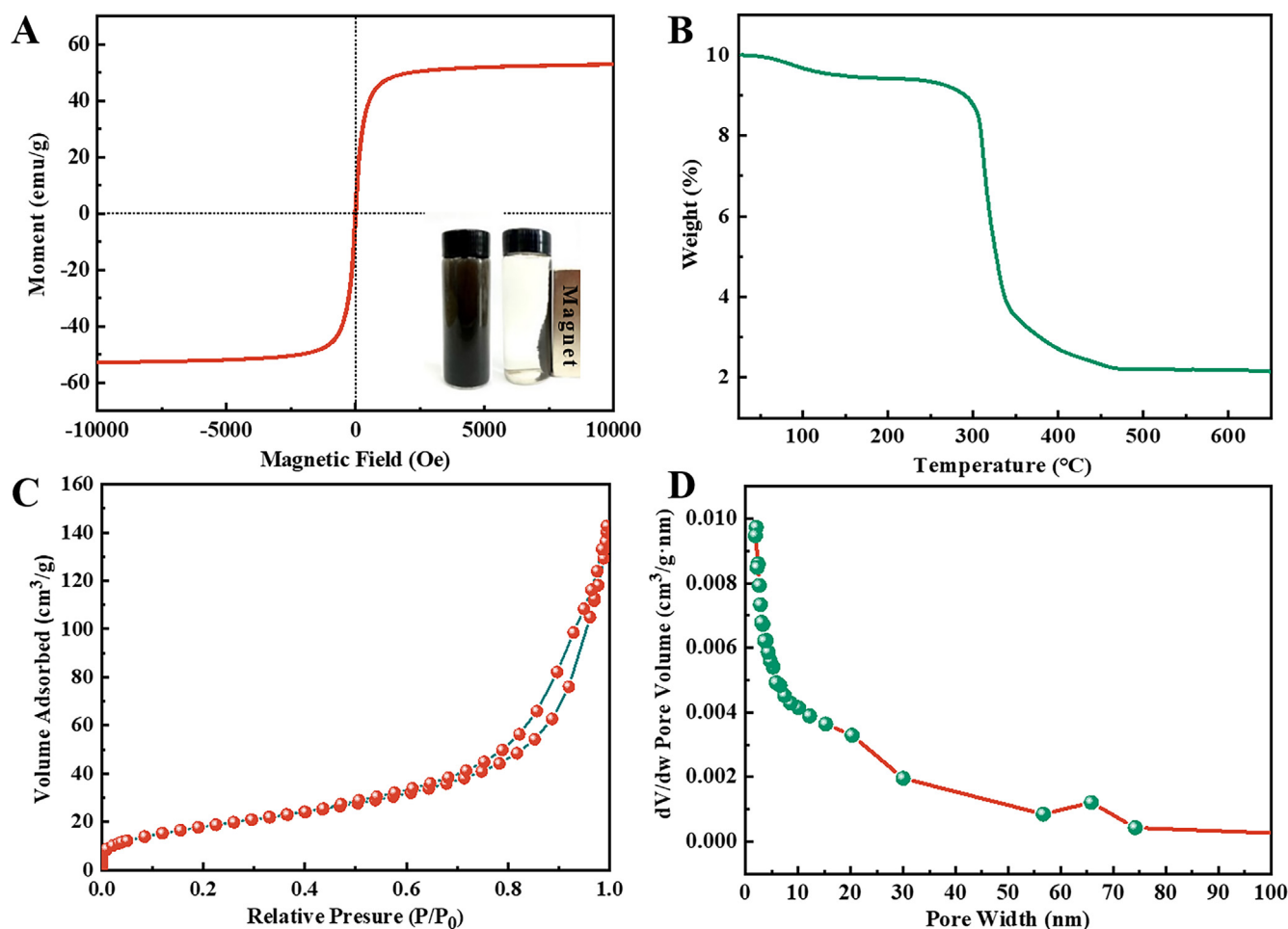
Fig. 2 (A) Magnetic hysteresis loops of Fe_3O_4/Lp-biochar and the magnetic separation of adsorbent material (inset) through an external magnetic field. (B) TGA curve, (C) nitrogen adsorption–desorption isotherms and (D) pore-size distribution of the Fe_3O_4/Lp-biochar.

increased from 4.41 to 26.36 mg/g with the increasing MB concentrations (from 5 to 50 mg/L) (Fig. 3B), mainly due to increased collisions between adsorbent and adsorbed. Besides, the variation in the efficiency of MB removal by the Fe_3O_4/Lp-biochar adsorbent according to adsorption time is shown in Fig. 3C. The adsorption capacity changed over time in three stages. In the initial stages of adsorption (0 ~ 30 min), the Fe_3O_4/Lp-biochar presented a sharp increase in the adsorption capacity, attributed to a considerable amount of adsorption sites. With contact time extension, the adsorption sites decreased gradually and the adsorption amount of MB increased slowly in the second stage. The third adsorption stage occurred after 60 min and the reaction system had reached adsorption equilibrium. Although the equilibrium time varied for different initial MB concentrations, adsorption equilibrium experiments were conducted for 90 min.

To examine the effect of temperature on adsorption efficiency, the adsorption capacity of Fe_3O_4/Lp-biochar for MB at different temperatures was further compared. The equilibrium capacity of MB increased first then decreased with increasing temperatures (Fig. 3D), possibly because the electrostatic interactions change with the temperature. The optimum temperature for MB adsorption by Fe_3O_4/Lp-biochar

was 25 °C. Moreover, the optimal adsorbent addition amount was chosen to be 0.10 mg/mL in this study.

3.4. Adsorption kinetics

To study the adsorption process, the kinetic data were analyzed using the pseudo-first-order and pseudo-second-order models, respectively. The adsorption kinetics and fitting parameters for the obtained data of Fe_3O_4/Lp-biochar for MB removal are presented in Fig. 4A and B. The R^2 of the pseudo-second-order kinetic was higher than the pseudo-first-order kinetic (Table 1), and its calculated equilibrium adsorption capacity ($q_{e,cal}$) was also very close to the experimental equilibrium adsorption capacity ($q_{e,exp}$). These results indicated that the adsorption behavior of the Fe_3O_4/Lp-biochar for MB removal fitted better the pseudo-second-order kinetic model and suggested that the adsorption was due to chemisorption or chemical adsorption (Shen et al., 2019). Moreover, the k_2 values of the pseudo-second-order model decreased from 0.04633 to 0.01811 (g mg^{-1} min^{-1}) with the increase of MB concentrations from 5 to 20 mg/L, indicating that the driving force between dye molecules and adsorbent can be markedly improved by increasing the initial MB concentration.
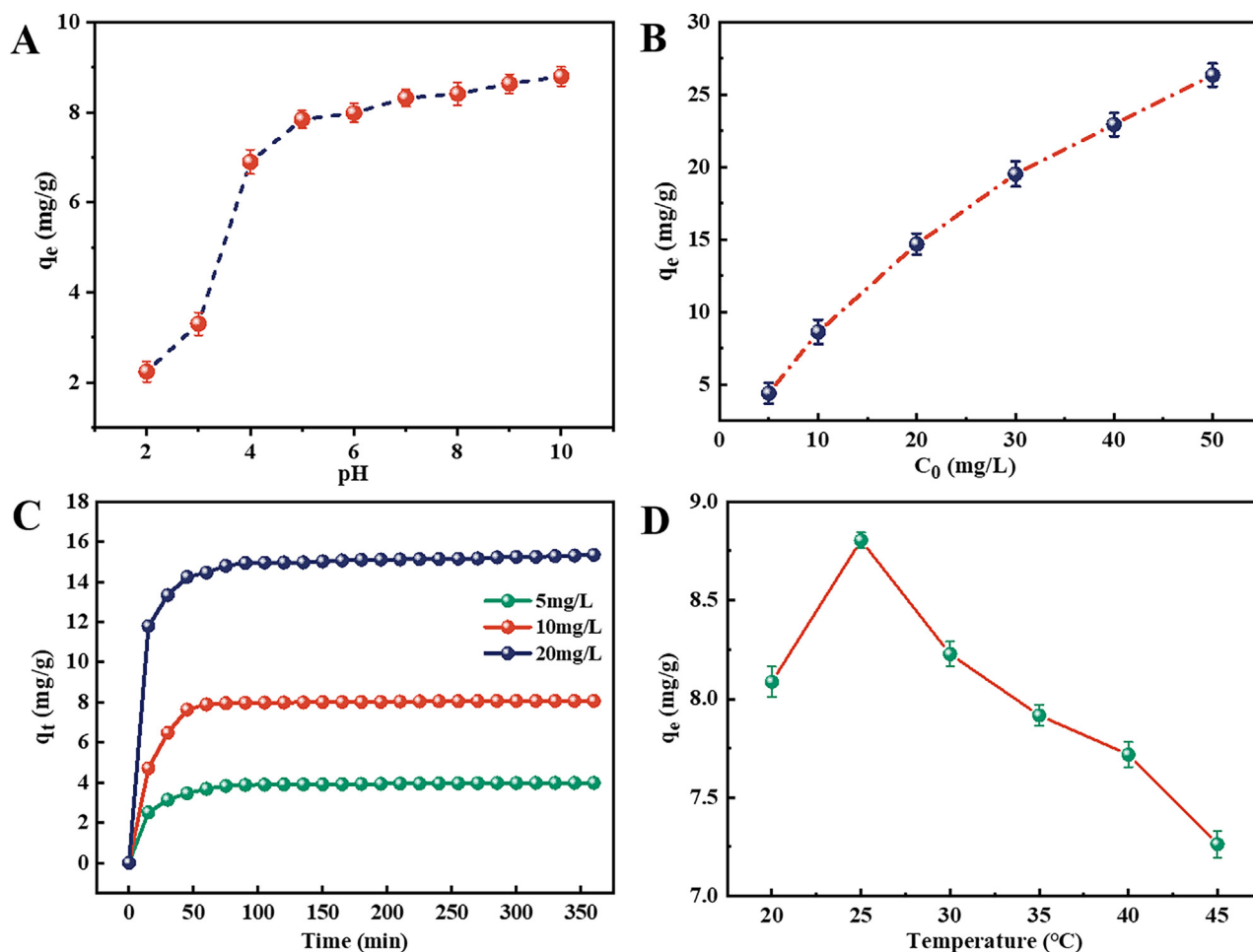
Fig. 3 Effects of (A) solution pH, (B) initial MB concentration, (C) contact time and (D) reaction temperature on adsorption efficiency of the Fe_3O_4/Lp-biochar.

Besides, the Weber-Morris model was also used to analyze whether the adsorption rate was controlled by outer diffusion or inner diffusion or both. Plots of q_t against $t_{1/2}$ and the linear regression of q_t versus $t_{1/2}$ are shown in Fig. 4C, and the corresponding kinetic parameters are listed in Table 2. The adsorption process of the Fe_3O_4/Lp-biochar could be divided into two stages. In the initial stage, the sharper slope can be explained by the boundary layer effect (Ma et al., 2015), which mainly involves the transportation of dye molecules from the aqueous solution to the surface of the Fe_3O_4/Lp-biochar adsorbent. The second stage indicated intraparticle diffusion of dye molecules through abundant active sites of the biochar adsorbent. The calculated k_1 was significantly higher than k_2, suggesting that the mass transfer was quicker than the intraparticle diffusion. The results indicated that the overall adsorption process of the Fe_3O_4/Lp-biochar might be jointly controlled by external mass transfer and intraparticle diffusion. Additionally, intraparticle diffusion was not the rate-limiting step since the c_2 values were not equal to zero (Chen et al., 2014).

3.5. Adsorption isotherms

To clarify the equilibrium adsorption characteristics of MB onto Fe_3O_4/Lp-biochar, the classic Langmuir and Freundlich

isotherm models were applied to fit the obtained equilibrium adsorption data. The Langmuir and Freundlich isothermal models are presented in Fig. 4D, and the corresponding parameters calculated from the nonlinear fit by both models are listed in Table 3. Both isothermal models fit well with adsorption data ($R^2 > 0.95$). Nevertheless, the R^2 value of the Langmuir model ($R^2 = 0.9669$) was lower than the Freundlich model ($R^2 = 0.9905$), suggesting the highly heterogeneous distribution of adsorption energy and the existence of intermolecular interactions between MB and Fe_3O_4/Lp-biochar. Therefore, the Freundlich adsorption isotherm model can more accurately describe the adsorption of MB by Fe_3O_4/Lp-biochar adsorption than the Langmuir isotherm model. The Freundlich constant n was higher than 1.0, confirming that the adsorbent had a favorable adsorption performance for dye molecules (Fan et al., 2012). These results also indicated that the adsorption of MB by Fe_3O_4/Lp-biochar was mainly based on multi-molecular layer adsorption (Zhang et al., 2020). These obtained results indicated that the adsorption of Fe_3O_4/Lp-biochar toward MB is a complex physicochemical process involving possible charge-transfer-mediated chemical reactions. The remarkable adsorption capacity of as-prepared biochar adsorbent might be ascribed to the synergetic effects of its unique surface structure and micropore con-
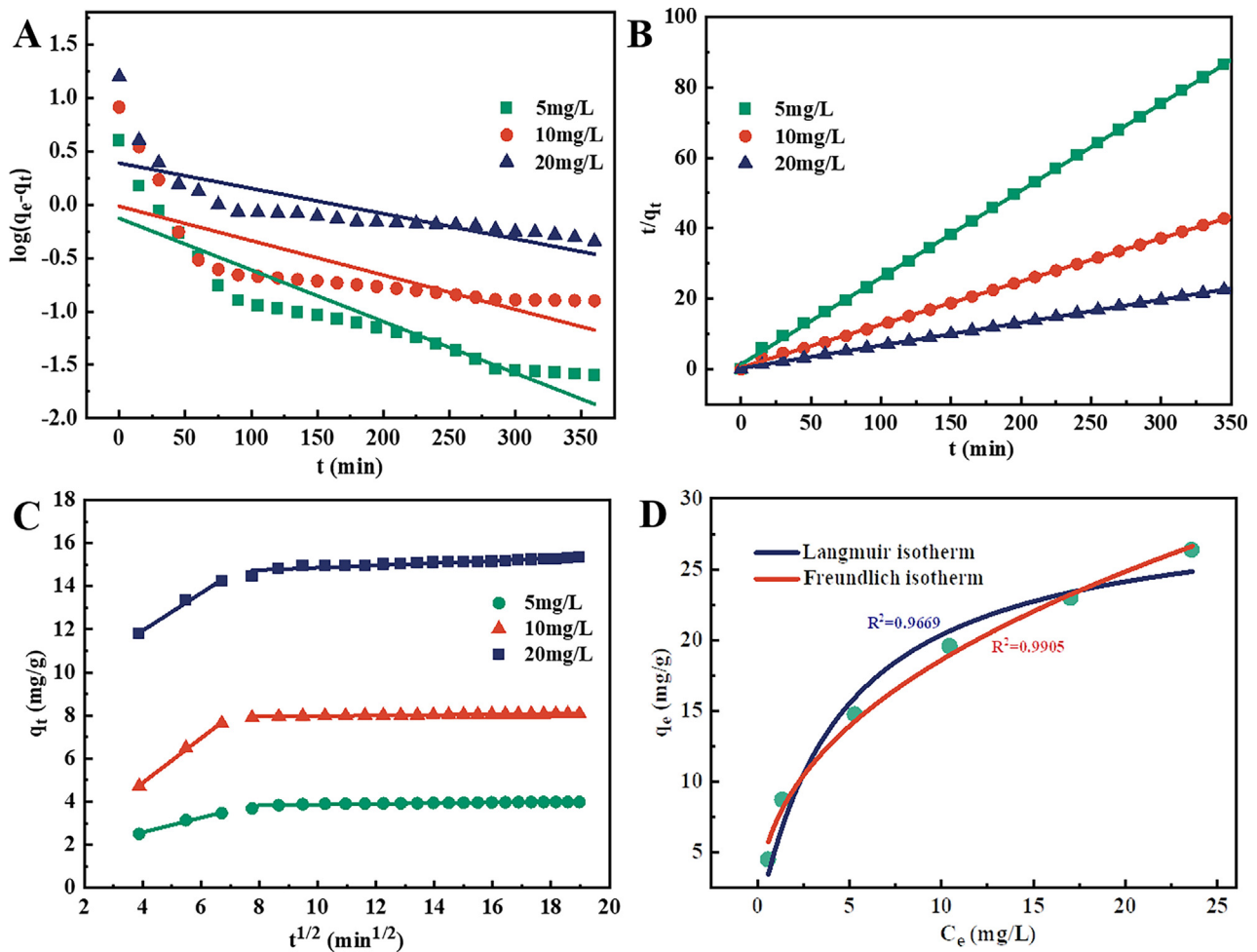
Fig. 4 (A) Pseudo-first-order kinetics, (B) pseudo-second-order kinetics, (C) intraparticle diffusion kinetics and (D) equilibrium isotherms of MB adsorption on the Fe_3O_4/Lp-biochar.

Table 1 Kinetic model parameters of MB adsorption on the Fe_3O_4/Lp-biochar.

C_0 (mg/L)	$q_{e, exp}$ (mg/g)	Pseudo-first-order-kinetics			Pseudo-second-order-kinetics		
		$q_{e, cal}$ (mg/g)	k_1 (min^{-1})	R^2	$q_{e, cal}$ (mg/g)	k_2 (g min^{-1} min^{-1})	R^2
5	4.01	0.75	0.0111	0.8266	4.05	0.0463	0.9998
10	8.20	0.97	0.0111	0.5536	8.18	0.0330	0.9997
20	15.80	2.45	0.0055	0.5867	15.42	0.0181	0.9999

Table 2 Intraparticle diffusion model parameters of MB adsorption on the Fe_3O_4/Lp-biochar.

C_0 (mg/L)	First stage			Second stage		
	k_1 (mg g^{-1}h$^{-1/2}$)	c_1 (mg/g)	R^2	k_2 (mg g^{-1}h$^{-1/2}$)	c_2 (mg/g)	R^2
5	0.3411	1.2147	0.9787	0.0174	3.6841	0.7285
10	1.0360	0.7373	0.9959	0.0134	7.8385	0.9194
20	0.8694	8.4682	0.9889	0.0537	14.3237	0.8512

Table 3   Isotherm parameters of MB adsorption on the Fe_3O_4/Lp-biochar.

Langmuir			Freundlich		
b (L/mg)	q_m (mg/g)	R^2	k	n	R^2
0.2198	29.6156	0.9669	7.1018	2.3932	0.9905
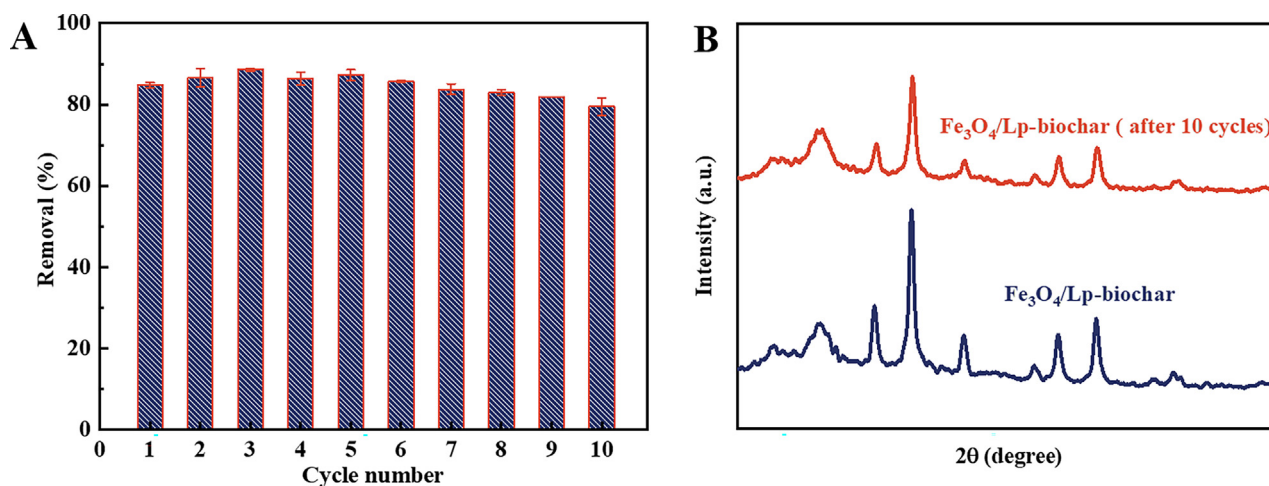
Fig. 5   (A) Cycling performance of the Fe_3O_4/Lp-biochar for MB removal. (B) XRD patterns of the Fe_3O_4/Lp-biochar without adsorption and with MB adsorption after 10 adsorption–desorption cycles.

tent, the electrostatic interaction between chemicals and the adsorbent, as well as the functional groups on the surface of the carbon material.

3.6. Reusability of the Fe_3O_4/Lp-biochar

The reusability of adsorbent materials is vital to cost savings in practical applications. Thus, we evaluated whether the Fe_3O_4/Lp-biochar retains its high MB adsorption capacity after 10 adsorption–desorption cycles. The MB adsorption efficiency only decreased by only 5.28% even after 10 cycles under the same experimental conditions (Fig. 5A), demonstrating that the as-synthesized biochar adsorbent has excellent cyclic performance. Furthermore, no evident changes occurred in the surface morphology and crystal structure (Fig. 5B) of the Fe_3O_4/Lp-biochar after 10 adsorption–desorption cycles. Therefore, the prepared Fe_3O_4/Lp-biochar nanocomposites have excellent reusability and adsorptive properties.

4. Conclusions

In summary, a new magnetic biochar derived from lemon peel residue, denoted as Fe_3O_4/Lp-biochar, was easily prepared at low temperature by a one-step hydrothermal method. The as-obtained magnetic nanocomposites exhibited excellent magnetic recovery characteristics and showed good adsorption properties for methylene blue (MB). The maximum MB adsorption capacity of 26.36 mg/g by the Fe_3O_4/Lp-biochar can be achieved under the optimal experimental conditions, and the MB removal efficiency was maintained at 94.7% after 10 cycles of use. Kinetic studies have shown that the adsorption of MB on the Fe_3O_4/Lp-biochar can be well fitted Pseudo-second-order kinetic and Freundlich isotherm models. The adsorption mechanism

involves mainly physical and chemisorption processes. The results demonstrate that biochar adsorbents derived from lemon peels show great promise in addressing chemical pollutants and also offer new opportunities for recycling these biological wastes.

Declaration of Competing Interest

The authors declare that they have no known competing financial interests or personal relationships that could have appeared to influence the work reported in this paper.

Acknowledgements

References

Albishri, W.S., Katouah, H.A., 2023. Functionalization of sodium magnesium silicate hydroxide/sodium magnesium silicate hydrate nanostructures by chitosan as a novel nanocomposite for efficient removal of methylene blue and crystal violet dyes from aqueous media. Arabian J. Chem. 16,. https://doi.org/10.1016/j.arabjc.2023.104804 104804.

Awasthi, M.K., 2022. Engineered biochar: A multifunctional material for energy and environment. Environ. Pollut. 298,. https://doi.org/10.1016/j.envpol.2022.118831 118831.

Behin, J., Farhadian, N., 2017. Response surface methodology for ozonation of trifluralin using advanced oxidation processes in an airlift photoreactor. Appl. Water Sci. 7, 3103–3112. https://doi.org/10.1007/s13201-016-0443-y.

Benjelloun, M., Miyah, Y., Akdemir Evrendilek, G., et al, 2021. Recent advances in adsorption kinetic models: Their application to

dye types. Arabian J. Chem. 14,. https://doi.org/10.1016/j.arabjc.2021.103031 103031.

Bhattacharya, K., Parasar, D., Mondal, B., et al, 2015. Mesoporous magnetic secondary nanostructures as versatile adsorbent for efficient scavenging of heavy metals. Sci. Rep. 5, 17072. https://doi.org/10.1038/srep17072.

Chae, H.S., Piao, S.H., Choi, H.J., 2015. Fabrication of spherical Fe_3O_4 particles with a solvothermal method and their magnetorheological characteristics. J. Ind. Eng. Chem. 29, 129–133. https://doi.org/10.1016/j.jiec.2015.02.027.

Chen, Z., Fu, J., Wang, M., et al, 2014. Adsorption of cationic dye (methylene blue) from aqueous solution using poly(cyclotriphosphazene-co-4,4′-sulfonyldiphenol) nanospheres. Appl. Surf. Sci. 289, 495–501. https://doi.org/10.1016/j.apsusc.2013.11.022.

Davoodbeygi, Y., Askari, M., Salehi, E., et al, 2023. A review on hybrid membrane-adsorption systems for intensified water and wastewater treatment: Process configurations, separation targets, and materials applied. J. Environ. Manage. 335,. https://doi.org/10.1016/j.jenvman.2023.117577 117577.

Ebrahimzadeh, H., Behbahani, M., 2017. A novel lead imprinted polymer as the selective solid phase for extraction and trace detection of lead ions by flame atomic absorption spectrophotometry: Synthesis, characterization and analytical application. Arabian J. Chem. 10, S2499–S2508. https://doi.org/10.1016/j.arabjc.2013.09.017.

El Hamdouni, Y., El Hajjaji, S., Szabó, T., et al, 2022. Biomass valorization of walnut shell into biochar as a resource for electrochemical simultaneous detection of heavy metal ions in water and soil samples: Preparation, characterization, and applications. Arabian J. Chem. 15,. https://doi.org/10.1016/j.arabjc.2022.104252 104252.

Fan, W., Gao, W., Zhang, C., et al, 2012. Hybridization of graphene sheets and carbon-coated Fe_3O_4 nanoparticles as a synergistic adsorbent of organic dyes. J. Mater. Chem. 22, 25108–25115. https://doi.org/10.1039/C2JM35609K.

Ghabaee, S., Behin, J., Ansari, M., et al, 2020. Synthesis and characterization maleate-alumoxane nanoparticles for removal of reactive yellow 84 dye from aqueous solution. Adv. Powder Technol. 31, 2061–2071. https://doi.org/10.1016/j.apt.2020.02.040.

Harindintwali, J.D., He, C., Xiang, L., et al, 2023. Effects of ball milling on biochar adsorption of contaminants in water: A meta-analysis. Sci. Total Environ. 882,. https://doi.org/10.1016/j.scitotenv.2023.163643 163643.

Ivanova, N.V., Trofimova, N.N., Es'kova, L.A., et al, 2012. The study of the reaction of Pectin-Ag(0) nanocomposites formation. Int. J. Carbohydr. Chem. 2012,. https://doi.org/10.1155/2012/459410 459410.

Jiang, H., Zhang, W., Xu, Y., et al, 2022. An advance on nutritional profile, phytochemical profile, nutraceutical properties, and potential industrial applications of lemon peels: A comprehensive review. Trends Food Sci. Technol. 124, 219–236. https://doi.org/10.1016/j.tifs.2022.04.019.

Jung, K.-W., Choi, B.H., Jeong, T.-U., et al, 2016. Facile synthesis of magnetic biochar/Fe_3O_4 nanocomposites using electro-magnetization technique and its application on the removal of acid orange 7 from aqueous media. Bioresour. Technol. 220, 672–676. https://doi.org/10.1016/j.biortech.2016.09.035.

Kant Bhatia, S., Palai, A.K., Kumar, A., et al, 2021. Trends in renewable energy production employing biomass-based biochar. Bioresour. Technol. 340,. https://doi.org/10.1016/j.biortech.2021.125644 125644.

Kyomugasho, C., Willemsen, K.L.D.D., Christiaens, S., et al, 2015. Pectin-interactions and in vitro bioaccessibility of calcium and iron in particulated tomato-based suspensions. Food Hydrocolloids 49, 164–175. https://doi.org/10.1016/j.foodhyd.2015.03.011.

Lan, S., Leng, Z., Guo, N., et al, 2014. Sesbania gum-based magnetic carbonaceous nanocomposites: Facile fabrication and adsorption

behaviour. Colloids Surf. A 446, 163–171. https://doi.org/10.1016/j.colsurfa.2014.01.054.

Liu, M., Zhang, P., Qu, Z., et al, 2019. Conductive carbon nanofiber interpenetrated graphene architecture for ultra-stable sodium ion battery. Nat. Commun. 10, 3917. https://doi.org/10.1038/s41467-019-11925-z.

Ma, J., Yang, M., Yu, F., et al, 2015. Water-enhanced removal of ciprofloxacin from water by porous graphene hydrogel. Sci. Rep. 5, 13578. https://doi.org/10.1038/srep13578.

Mao, G.-Y., Yang, W.-J., Bu, F.-X., et al, 2014. One-step hydrothermal synthesis of Fe_3O_4@C nanoparticles with great performance in biomedicine. J. Mater. Chem. B 2, 4481–4488. https://doi.org/10.1039/C4TB00394B.

Nabilah, B., Purnomo, A.S., Prasetyoko, D., et al, 2023. Methylene Blue biodecolorization and biodegradation by immobilized mixed cultures of Trichoderma viride and Ralstonia pickettii into SA-PVA-Bentonite matrix. Arabian J. Chem. 16,. https://doi.org/10.1016/j.arabjc.2023.104940 104940.

Peng, Y., Azeem, M., Li, R., et al, 2022. Zirconium hydroxide nanoparticle encapsulated magnetic biochar composite derived from rice residue: Application for As(III) and As(V) polluted water purification. J. Hazard. Mater. 423,. https://doi.org/10.1016/j.jhazmat.2021.127081 127081.

Pourzad, A., Sobhi, H.R., Behbahani, M., et al, 2020. Efficient visible light-induced photocatalytic removal of paraquat using N-doped TiO_2@SiO_2@Fe_3O_4 nanocomposite. J. Mol. Liq. 299,. https://doi.org/10.1016/j.molliq.2019.112167 112167.

Pu, J., Shen, L., Zhu, S., et al, 2014. Fe_3O_4@C core–shell microspheres: synthesis, characterization, and application as supercapacitor electrodes. J. Solid State Electrochem. 18, 1067–1076. https://doi.org/10.1007/s10008-013-2359-x.

Qu, J., Akindolie, M.S., Feng, Y., et al, 2020. One-pot hydrothermal synthesis of NaLa(CO3)2 decorated magnetic biochar for efficient phosphate removal from water: Kinetics, isotherms, thermodynamics, mechanisms and reusability exploration. Chem. Eng. J. 394,. https://doi.org/10.1016/j.cej.2020.124915 124915.

Qu, J., Shi, J., Wang, Y., et al, 2022. Applications of functionalized magnetic biochar in environmental remediation: A review. J. Hazard. Mater. 434,. https://doi.org/10.1016/j.jhazmat.2022.128841 128841.

Shen, X., Huang, P., Li, F., et al, 2019. Compressive Alginate Sponge Derived from Seaweed Biomass Resources for Methylene Blue Removal from Wastewater. Polymers (Basel) 11. https://doi.org/10.3390/polym11060961.

Sobhi, H.R., Mohammadzadeh, F., Behbahani, M., et al, 2022. Application of a modified MWCNT-based d-μSPE procedure for determination of bisphenols in soft drinks. Food Chem. 385,. https://doi.org/10.1016/j.foodchem.2022.132644 132644.

Sutarut, P., Cheirsilp, B., Boonsawang, P., 2023. The potential of oil palm frond biochar for the adsorption of residual pollutants from real latex industrial wastewater. Int. J. Environ. Res. 17, 16. https://doi.org/10.1007/s41742-022-00503-9.

Wu, Y., Lu, H., Thanh, N.C., et al, 2023. Mixed pollutants adsorption potential of Eichhornia crassipes biochar on Manihot esculenta processing industry effluents. Environ. Res. 231,. https://doi.org/10.1016/j.envres.2023.116074 116074.

Xuan, S., Hao, L., Jiang, W., et al, 2007. A facile method to fabricate carbon-encapsulated Fe_3O_4 core/shell composites. Nanotechnology 18,. https://doi.org/10.1088/0957-4484/18/3/035602 035602.

Yin, G., Chen, X., Sarkar, B., et al, 2023. Co-adsorption mechanisms of Cd(II) and As(III) by an Fe-Mn binary oxide biochar in aqueous solution. Chem. Eng. J. 466,. https://doi.org/10.1016/j.cej.2023.143199 143199.

Zhang, H., Tu, Y.-J., Duan, Y.-P., et al, 2020. Production of biochar from waste sludge/leaf for fast and efficient removal of diclofenac. J. Mol. Liq. 299,. https://doi.org/10.1016/j.molliq.2019.112193 112193.

Zhang, W., Zhang, L.Y., Zhao, X.J., et al, 2016. Citrus pectin derived ultrasmall $Fe_3O_4@C$ nanoparticles as a high-performance adsorbent toward removal of methylene blue. J. Mol. Liq. 222, 995–1002. https://doi.org/10.1016/j.molliq.2016.07.144.

Zhou, S., Du, Z., Li, X., et al, 2019. Degradation of methylene blue by natural manganese oxides: kinetics and transformation products. R. Soc. Open Sci. 6,. https://doi.org/10.1098/rsos.190351 190351.